Supplementary information

# The Synthesis, Structure and Electronic Properties of a Lead-Free Hybrid Inorganic-Organic Double Perovskite $(MA)_2KBiCl_6$ (MA = methylammonium)

Fengxia Wei,[a] Zeyu Deng,[a] Shijing Sun,[a] Fei Xie,[a] Gregor Kieslich,[a] Donald M. Evans,[b] Michael A. Carpenter[b] Paul D. Bristowe[a] and Anthony K. Cheetham[a]*

[a] Department of Materials Science and Metallurgy, University of Cambridge, 27 Charles Babbage Road, CB3 0FS, United Kingdom

[b] Department of Earth Sciences, University of Cambridge, S109 Downing Street, CB2 3EQ, United Kingdom

**Table of Contents:**

Figure S9 (a) Nanoindentation plane (purple) and direction (blue arrow) (b) Calculated 3D directional Young's modulus of $(MA)_2KBiCl_6$ and its contour plot on (c) (001) plane (d) (010) plane and (e) the plane perpendicular to [100]. Nano-indentation Young's modulus is shown as a red dot in (d) and (e) along c-axis compared with DFT results (blue curve). Units shown are in GPa.

Figure S10. Variation of $f^2$ (proportional to elastic constants) and $Q^{-1}$ (indicative of acoustic attenuation) from selected resonance peaks in RUS spectra collected during cooling (blue) and heating (red). There is clear evidence of a phase transition at ~260 K, with a step in $f^2$ and peak in $Q^{-1}$ occurring at 260 K during cooling and 267 K during heating.

Figure S11 Comparison of the band structure of $(MA)_2KBiCl_6$ (a) with and (b) without considering spin-orbit coupling (SOC). Band gap drops around 0.78 eV compared with 1.08 eV for $MAPbI_3$ in previous study. The following high symmetry points in the first Brillouin zone were used: Γ (0,0,0), A (0,0,0.5), H (-0.333,0.667,0.5), K (-0.333,0.667,0), M (0,0.5,0)

Table S1. Atomic coordinates for $(MA)_2KBiCl_6$ obtained from single crystal diffraction compared with values from DFT geometry optimization. Atomic labels are shown in Figure S8.

Table S2. Anisotropic displacement parameters ($Å^2$) for $(MA)_2KBiCl_6$.

Table S3. Interatomic distances for $(MA)_2KBiCl_6$ from experiments compared with DFT.

Table S4. Bond angles for $(MA)_2KBiCl_6$ from experiments compared with DFT.

Table S5. Single crystal X-ray diffraction experimental details.

Table S6. DFT calculated single crystal elastic stiffness constants ($C_{ij}$) and elastic properties of bulk modulus (B), shear modulus (G), Young's modulus (E) and Poisson's ratio (ν). Except ν, all the units are in GPa.

## Experimental details:

Crystal structure determination was carried out using an Oxford Gemini E Ultra diffractometer, Mo Kα radiation (λ = 0.71073Å), equipped with an Eos CCD detector. Data collection and reduction were conducted using CrysAliPro (Agilent Technologies). An empirical absorption correction was applied with the Olex2 platform,[1] and the structure was solved using ShelXT[2] and refined by ShelXL.[3] Phase purity was confirmed by powder X-ray diffraction (PXRD, Bruker D8 diffractometer with primary Ni filter). Lattice parameters obtained from a Pawley fit performed using TOPAS4.1[4] are in good agreement with lattice parameter from single crystal X ray diffraction. No secondary phase was detected for products synthesised by both solution precipitation and hydrothermal methods (Figure S2).

Optical measurements were carried out on a PerkinElmer Lambda 750 UV-Visible spectrometer in the reflectance mode with a 2nm slit width. The scan interval was 1 nm and the scan range was between 200 and 1500nm. The measurement was repeated by rotating the sample holder by 90° to ensure that the geometrical condition was fulfilled.

Nanoindentation experiments were performed at room temperature using an MTS NanoIndenter XP (MTS Corp., Eden Prairie, MN) located in an isolation cabinet in order to minimise the thermal instability and acoustic interference. With a dynamic displacement-controlled continuous stiffness measurement (CSM mode), as reported in previous literature,[5,6] indentations were carried out using a three-sided pyramidal Berkovich tip (radius ~100 nm) with the indenter aligned normal to the (001) plane of the single crystals. The Young's modulus (E) and indentation hardness (H) were obtained using the standard Oliver–Pharr Method.[7,8] Calibration was done using a fused silica standard with an elastic modulus of 72 GPa and hardness of 9 GPa. Poisson's ratio of the samples was assumed to be 0.3 in this model. Sample preparations followed the similar procedures of Sun *et. al.*.[9]

DFT calculations were performed using the Vienna *ab initio* Simulation Package (VASP).[10,11] Projector-augmented wave (PAW)[12] pseudopentials were used with the following valence electrons for each ion treated explicitly: Bi ($5d^{10}6s^{2}6p^{3}$), K ($3s^{2}3p^{6}4s^{1}$), Cl ($3s^{2}3p^{5}$), C ($2s^{2}2p^{2}$), N ($2s^{2}2p^{3}$) and H ($1s^{1}$). The semi-local van der Waals functional (vdW-DF) was used,[13] with the exchange energy calculated using the optimised optB86b generalised gradient approximation (GGA) functional. The correlation energy was obtained from the local density approximation (LDA) and the nonlocal correlation energy calculated from double space integration. A 500 eV planewave kinetic energy cutoff was used for all the calculations. For geometry optimisation a 4×4×2 Monkhorst-Pack[14] *k*-point mesh was employed, while for the electronic density of states (DOS) calculations a finer 5×5×2 mesh was used. The ions were relaxed until the forces on them were less than 0.01 eV/Å. Relativistic spin-orbit coupling (SOC) was included in the DOS and band structure calculations.

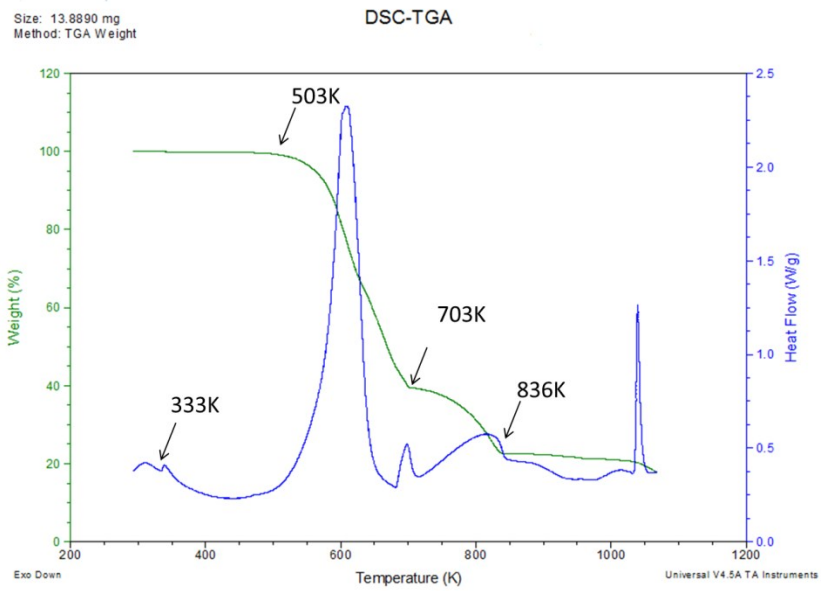


Figure S1. TGA and DSC curve for the $(MA)_2KBiCl_6$.

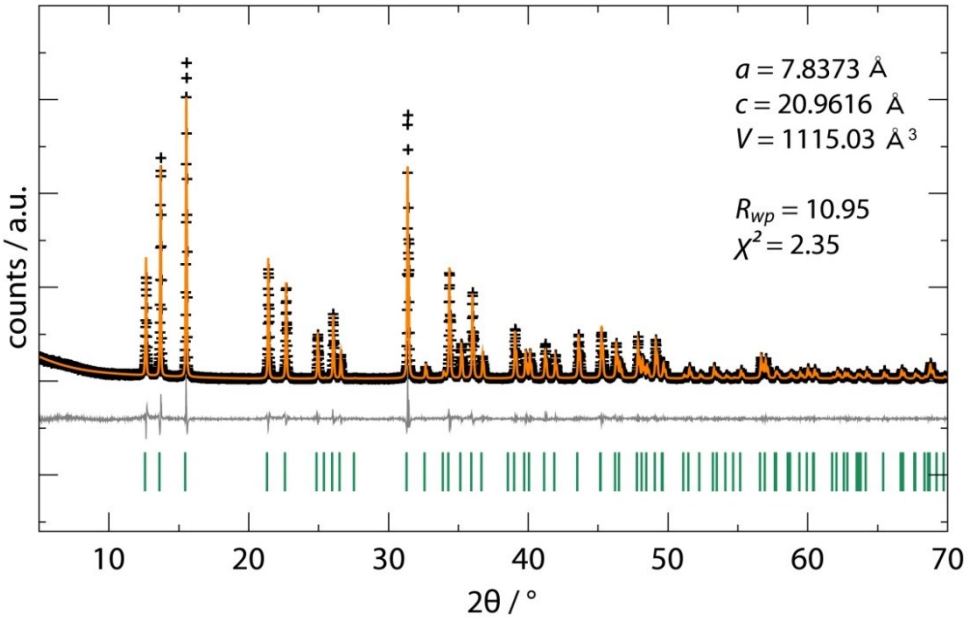


Figure S2. Powder X-ray diffraction pattern for $(MA)_2KBiCl_6$ and Pawley fit. The lattice parameters (inset) obtained from the Pawley fit agree well with lattice parameters from Single crystal X-ray diffraction. Blue - experimental, red – calculated, grey – differences between experimental and calculated curves. The tics where intensities are expected are shown in green.

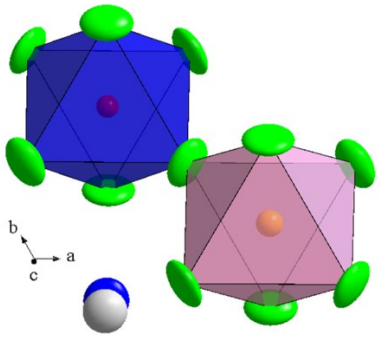


Figure S3. Ellipsoids for the Cl, C and N, viewed slightly away from *c* axis, drawn in 50% probability.

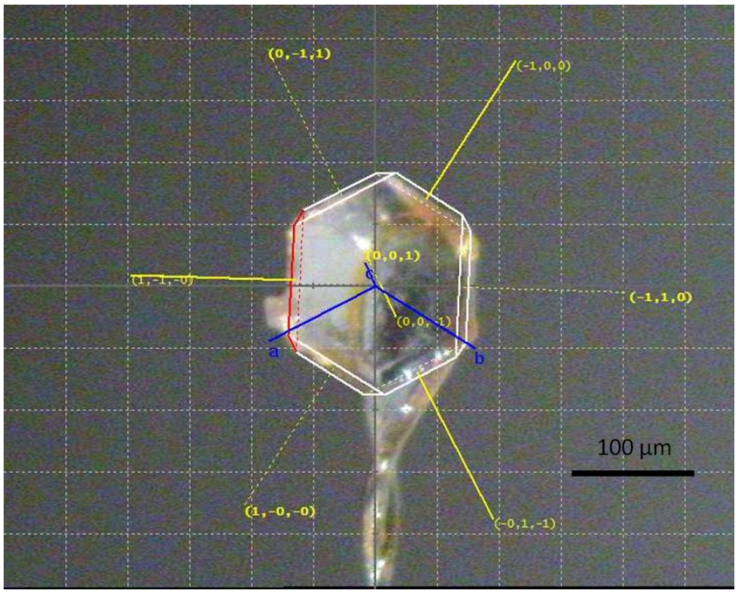


Figure S4. Photograph of $(MA)_2KBiCl_6$ with face indexing using single crystal X-ray diffraction.

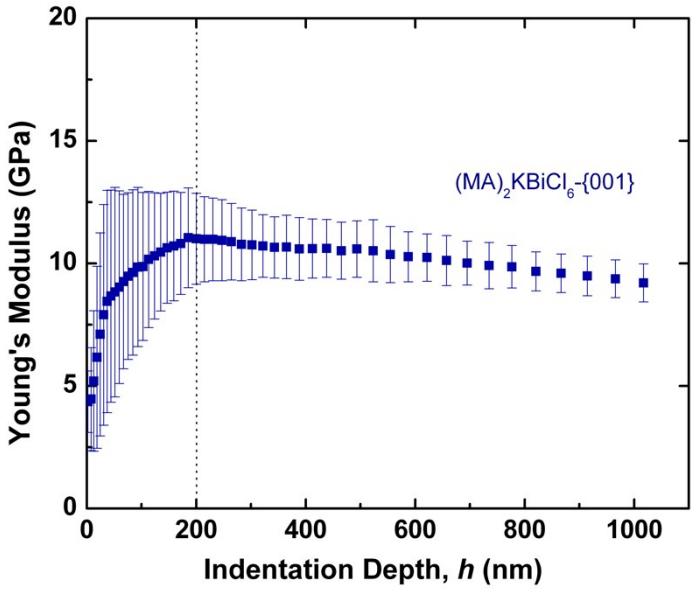


Figure S5. Young's modulus against indentation depth.

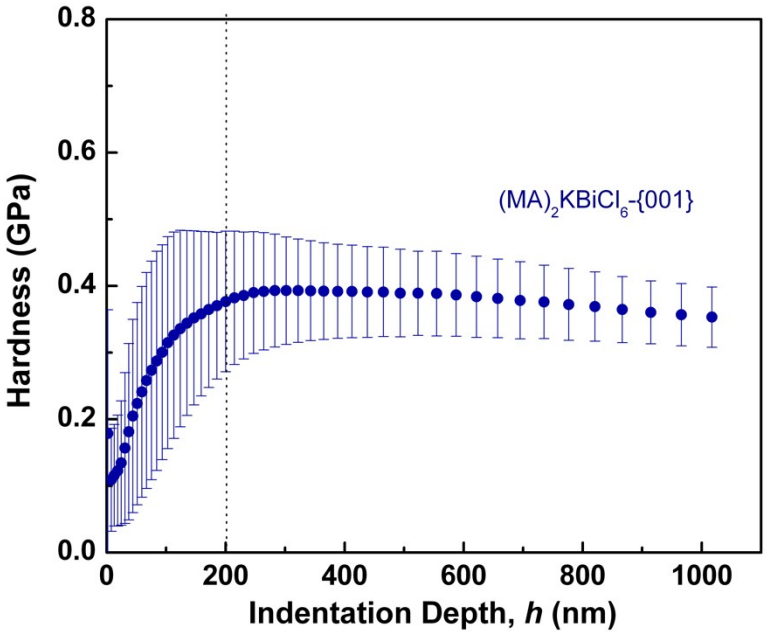


Figure S6. Hardness against indentation depth.

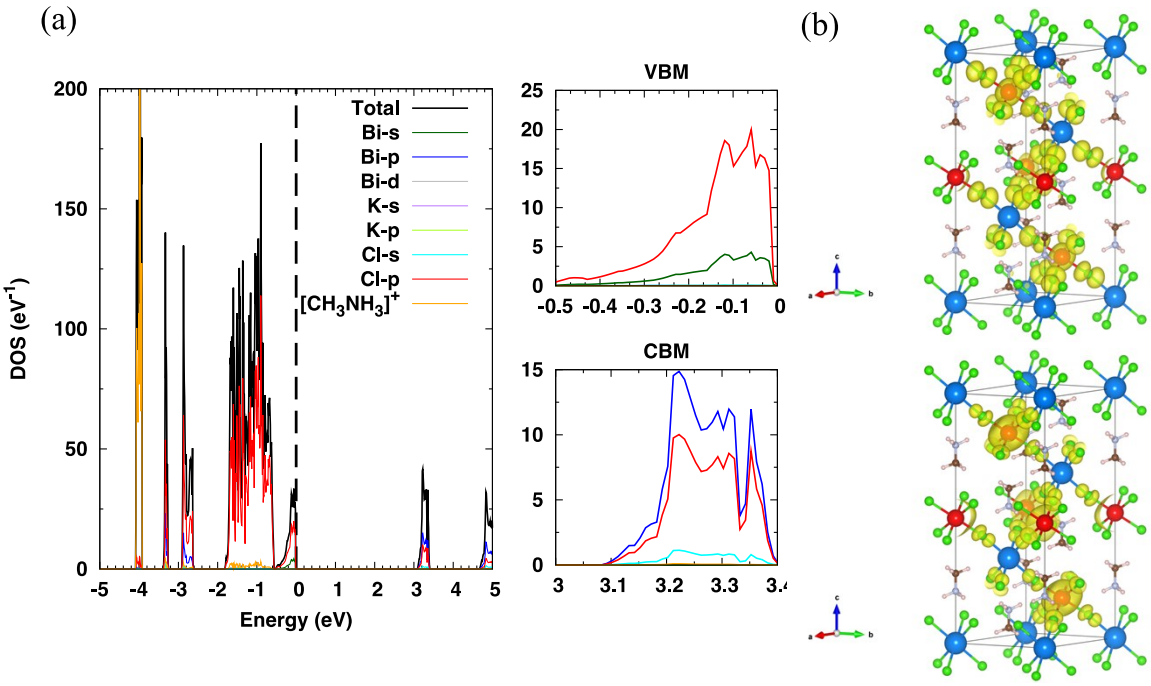


Figure S7 (a) Calculated total and partial density of states of $(MA)_2KBiCl_6$ (b) calculated band decomposed partial charge density (PCD) at the VBM (top) and the CBM (bottom).. The PCD is visualized using the VESTA program[15] and the electron isosurface level is set at 0.001 eV/Å$^3$. The density clouds are colored yellow and the atoms are: Bi-red, K-blue, Cl-green, C-brown, N-light blue and H-white.

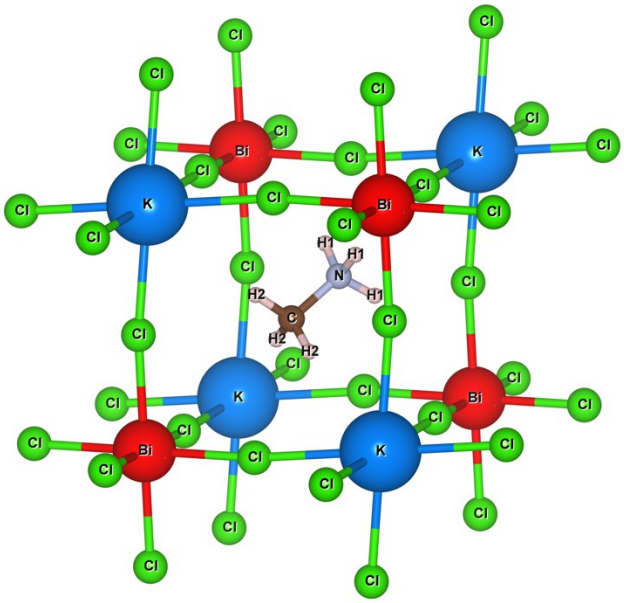


Figure S8. Atomic labels for $(MA)_2KBiCl_6$.

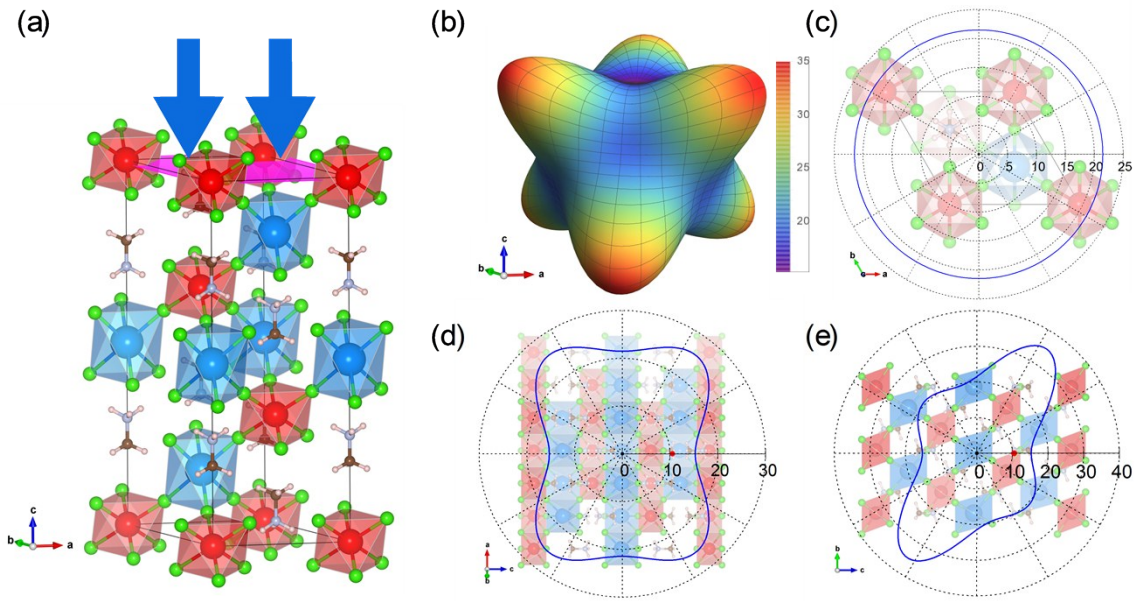


Figure S9 (a) Nanoindentation plane (purple) and direction (blue arrow) (b) Calculated 3D directional Young's modulus of $(MA)_2KBiCl_6$ and its contour plot on (c) (001) plane (d) (010) plane and (e) the plane perpendicular to [100]. Nano-indentation Young's modulus is shown as a red dot in (d) and (e) along c-axis compared with DFT results (blue curve). Units shown are in GPa.

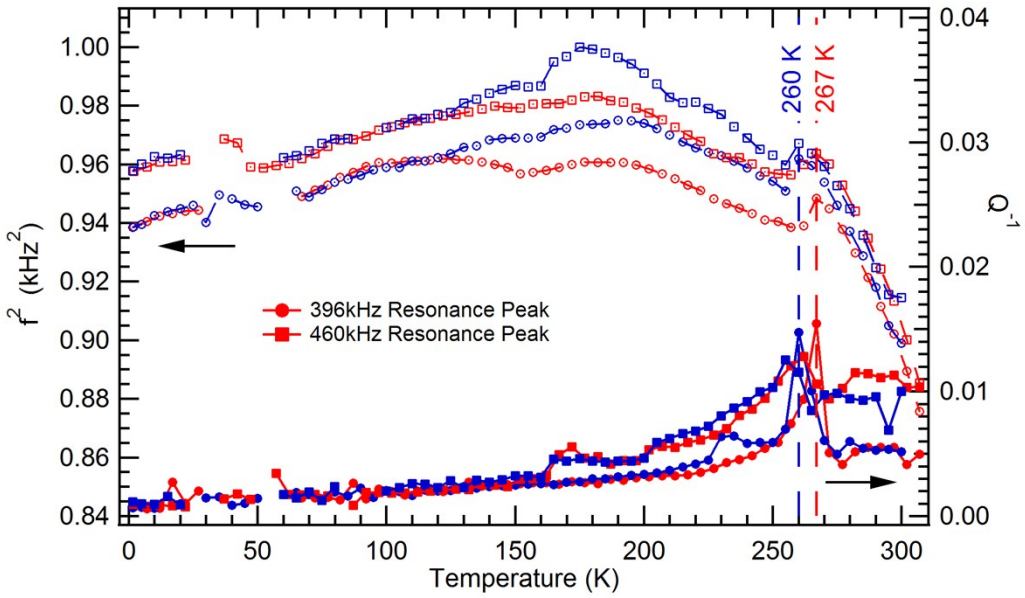


Figure S10. Variation of $f^2$ (proportional to elastic constants) and $Q^{-1}$ (indicative of acoustic attenuation) from selected resonance peaks in RUS spectra collected during cooling (blue) and heating (red). There is clear evidence of a phase transition at ~260 K, with a step in $f^2$ and peak in $Q^{-1}$ occurring at 260 K during cooling and 267 K during heating.

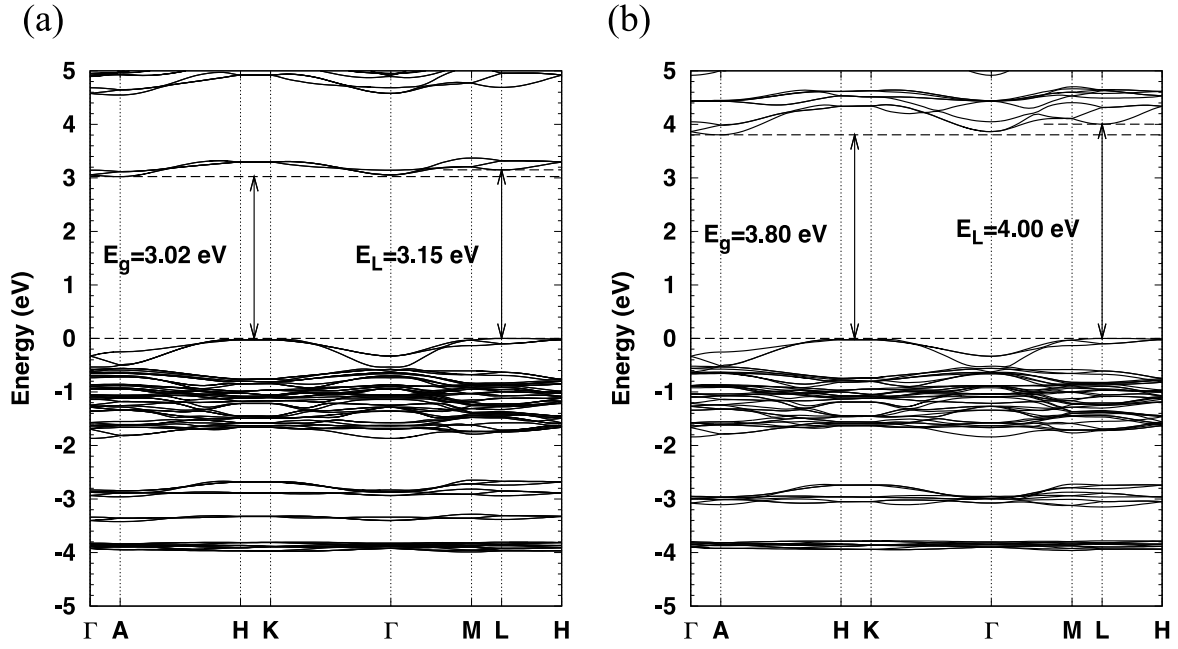


Figure S11 Comparison of the band structure of $(MA)_2KBiCl_6$ (a) with and (b) without considering spin-orbit coupling (SOC). Band gap drops around 0.78 eV compared with 1.08 eV for $MAPbI_3$ in previous study.[16] The following high symmetry points in the first Brillouin zone were used: Γ (0,0,0), A (0,0,0.5), H (-0.333,0.667,0.5), K (-0.333,0.667,0), M (0,0.5,0) and L (0,0.5,0.5). The band edges are found at L in the valence band and A in the conduction band.

Table S1. Atomic coordinates for $(MA)_2KBiCl_6$ obtained from single crystal diffraction compared with values from DFT geometry optimization. Atomic labels are shown in Figure S8.

| Atom | Experiments | | | | DFT | | |
|---|---|---|---|---|---|---|---|
| | x | y | z | Biso | x | y | z |
| Bi | 0.6667 | 0.3333 | 0.3333 | 0.0294(2) | 0.66667 | 0.33333 | 0.33333 |
| K | 0.3333 | 0.6667 | 0.1667 | 0.0364(7) | 0.33333 | 0.66667 | 0.16667 |
| Cl | 0.5029(2) | 0.4971(2) | 0.2619(1) | 0.105(1) | 0.50064 | 0.49936 | 0.26155 |
| C | 0.3333 | 0.6667 | 0.4456(9) | 0.121(9) | 0.33333 | 0.66667 | 0.44560 |
| N | 0.3333 | 0.6667 | 0.3815(8) | 0.133(8) | 0.33333 | 0.66667 | 0.37450 |
| H1 | - | - | - | - | 0.25664 | 0.74336 | 0.46244 |
| H2 | - | - | - | - | 0.40409 | 0.59591 | 0.35508 |

Table S2. Anisotropic displacement parameters (Å$^2$) for $(MA)_2KBiCl_6$.

| Atom | U11 | U22 | U33 | U23 | U13 | U12 |
|---|---|---|---|---|---|---|
| Bi | 0.0269(2) | 0.0269(2) | 0.0345(3) | 0 | 0 | 0.01345(11) |
| K | 0.0390(11) | 0.0390(11) | 0.0312(15) | 0 | 0 | 0.0195(5) |
| Cl | 0.145(2) | 0.145(2) | 0.0849(16) | 0.0203(7) | -0.0203(7) | 0.118(3) |
| C | 0.153(15) | 0.153(15) | 0.057(10) | 0 | 0 | 0.077(7) |
| N | 0.165(13) | 0.165(13) | 0.070(10) | 0 | 0 | 0.082(6) |

Table S3. Interatomic distances for $(MA)_2KBiCl_6$ from experiments compared with DFT.

| Atom 1 | Atom 2 | D (Å) | $D_{DFT}$ (Å) |
|---|---|---|---|
| Bi | Cl | 2.681(2) | 2.706 |
| K | Cl | 3.049(2) | 3.016 |
| N | C | 1.35(3) | 1.492 |
| C | H1 | - | 1.097 |
| N | H2 | - | 1.041 |
| H1 | Cl | - | 3.032 |
| H2 | Cl | - | 2.359 |
| N | Cl | 3.406(1) | 3.279 |
| C | Cl | 3.848(2) | 3.856 |

Table S4. Bond angles for $(MA)_2KBiCl_6$ from experiments compared with DFT.

| Bond Angle (°) | Exp | DFT |
|---|---|---|
| K-Cl-Bi | 173.04(12) | 172.51 |
| $Cl^1$-Bi-$Cl^2$ | 91.76(9) | 92.00 |
| $Cl^1$-Bi-$Cl^3$ | 88.24(9) | 88.00 |
| $Cl^5$-K1-$Cl^4$ | 98.33(9) | 98.86 |
| $Cl^4$-K1-$Cl^6$ | 81.67(9) | 81.14 |
| C-H1···Cl | - | 132.32 |
| N-H2···Cl | - | 146.70 |

Symmetry code: [1]1-y, x-y, z; [2]1+y, -x, z; [3] 4/3-x, 2/3-y, 2/3-z; [4] 2/3-x, 4/3-y, 1/3-z; [5] 1-y, 1+x-y, z; [6]2/3-y+x, 1/3+x, 1/3-z.

Table S5. Single crystal X-ray diffraction experimental details.

| | |
|---|---|
| Crystal data | |
| Chemical formula | $C_2N_2H_{12}KBiCl_6$ |
| Chemical formula weight | 524.9 |
| Temperature (K) | 300 |
| Cell Setting | R |
| Superspace group | $R\bar{3}m$ |
| *a* (Å) | 7.8372(2) |
| *c* (Å) | 20.9938 (2) |
| Volume (Å$^3$) | 1116.72(7) |
| Formula units (Z) | 3 |
| $D_x$ (Mg m$^{-3}$) | 2.288 |
| Crystal size (mm) | 0.0809 × 0.1048 × 0.1384 |
| Crystal colour | Colorless |
| | |
| Data collection | |
| Diffractometer | |
| Radiation type | Mo $K\alpha$ |
| Wavelength (Å) | 0.71073 |
| Absorption correction type | Analytical |
| Absorption coefficient μ (mm$^{-1}$) | 13.158 |
| Range of h, k, l | $-9\leq h\leq 7$, $-7\leq k\leq 9$, $-26\leq l\leq 26$ |
| No. of measured reflections | 1487 |
| No. of unique reflections | 316 |
| Criterion for observed reflections | $I > 2\sigma(I)$ |
| | |
| Refinement | |
| Refinement on | $F^2$ |
| *R, wR* (all reflections) | 0.0226, 0.0540 |
| S | 1.144 |
| No. of parameters | 17 |
| Weighting scheme | $w = [\sigma^2(F) + (0.01F)^2]^{-1}$ |
| $(\Delta/\text{s.u.})_{max}$ | 0.002 |
| $\Delta\rho_{max}$ (e Å$^{-3}$) | 0.65 |
| $\Delta\rho_{min}$ (e Å$^{-3}$) | -0.69 |
| Extinction correction | None |
| Source of atomic scattering factors | International Tables for Crystallography (1992, Vol.C)[17] |

Table S6. DFT calculated single crystal elastic stiffness constants ($C_{ij}$) and elastic properties of bulk modulus (B), shear modulus (G), Young's modulus (E) and Poisson's ratio (ν). Except ν, all the units are in GPa.

| Elastic Constants | $C_{11}$ | $C_{12}$ | $C_{13}$ | $C_{14}$ | $C_{33}$ | $C_{44}$ |
|---|---|---|---|---|---|---|
| | 31.75 | 11.75 | 14.38 | -3.58 | 24.79 | 12.11 |
| Elastic Properties | B | G | E | ν | | |
| | 18.75 | 6.27-14.79 | 15.28-35.18 | 0.10-0.50 | | |


1. O. V. Dolomano, L. J. Bourhis, R. J. Gildea, J.A.K. Howard and H. Puschmann, *J. Appl. Cryst*, 2009, **42**, 339-341.
2. G. M. Sheldrick, *Acta Cryst. A*, 2015, **71**, 3-8.
3. G. M. Sheldrick, *Acta Cryst. A*, 2008, **64**, 112-122.
4. Bruker, *TOPAS 4.1*, 2008.
5. J. Tan, C. Merrill, J. Orton and A. K. Cheetham, *Acta Mater.*, 2009, **57**, 3481-3496.
6. W. Li, S. Henke and A. K. Cheetham, *APL Mater.*, 2014, **2**, 123902.
7. W. C. Oliver and G. M. Pharr, *J. Mater. Res.*, 1992, **7**, 1564-1583.
8. W. C. Oliver and G. M. Pharr, *J. Mater. Res.*, 2004, **19**, 3-20.
9. S. Sun, Y. Fang, G. Kieslich, T. J. White and A. K. Cheetham, *J. Mater. Chem. A*, 2015, **3**, 18450-18455.
10. G. Kresse and J. Furthmuller, *Comp. Mater. Sci.*, 1996, **6**, 15-50.
11. G. Kresse and J. Furthmuller, *Phys. Rev. B*, 1996, **54**, 11169-11186.
12. P. E. Blochl, *Phys. Rev. B*, 1994, **50**, 17953-17979.
13. J. Klimes, D. R. Bowler and A. Michaelides, *Phys. Rev. B*, 2011, **83**, 195131.
14. H. J. Monkhorst and J. D. Pack, *Phys. Rev. B*, 1976, **13**, 5188-5192.
15. K. Momma and F. Izumi, *J Appl Crystallogr*, 2011, **44**, 1272-1276.
16. P. Umari, E. Mosconi and F. De Angelis, *Sci Rep-Uk*, 2014, **4**, 4467.
17. V. F. Sears, *International Tables for Crystallography*, Academic Publishers, Dordrecht, Kluwer, 1993.